Front motion and localized states in an asymmetric bistable activator-inhibitor system with saturation

Arik Yochelis[1] and Alan Garfinkel[1,2]

[1]*Department of Medicine (Cardiology), University of California, Los Angeles, CA 90095*
[2]*Department of Physiological Science, University of California, Los Angeles, CA 90095*

(Received March 20, 2008)

We study the spatiotemporal properties of coherent states (peaks, holes, and fronts) in a bistable activator-inhibitor system that exhibits biochemical saturated autocatalysis, and in which fronts do not preserve spatial parity symmetry. Using the Gierer-Meinhardt prototype model, we find the conditions in which two distinct pinning regions are formed. The first pinning type is known in the context of variational systems while the second is structurally different due to the presence of a heteroclinic bifurcation between two uniform states. The bifurcation also separates the parameter regions of counterpropagating fronts, leading in turn to the growth or contraction of activator domains. These phenomena expand the range of pattern formation theory and its biomedical applications: activator domain retraction suggests potential therapeutic strategies for patterned pathologies, such as cardiovascular calcification.

PACS numbers: 89.75.Kd, 47.20.Ky, 47.54.-r, 87.18.-h

Reaction-diffusion (RD) systems display many kinds of pattern formation, ranging from diverse stationary patterns to breathing and/or replicating spots and spiral waves [1]. One important application of RD systems is to biological pattern formation and morphogenesis, as originally suggested by Turing: reaction and diffusion of two chemical substances ("morphogens"), at different diffusion rates, can induce the spontaneous symmetry breaking of a homogeneous state and thus form patterns [2]. Turing described a simple activator-inhibitor system; since then, many model equations in physical, chemical, and biological contexts have been shown to form periodic patterns via a Turing-type instability [1, 3, 4]. There is a significant difference between chemical systems and biological media: In biology, the formation of labyrinthine patterns, for example, has been attributed to the phenomenon of *saturation* [3, 5].

Coherent states are another important property of spatially extended media [6]; we distinguish between *heteroclinic* orbits (fronts) and *homoclinic* orbits (localized states) in one-dimensional (1D) physical space. In the past, the formation of localized states in bistable systems was often linked to interactions between two front solutions [7]. However, this approach requires a large separation between two interacting fronts and thus is not valid for the analysis of spatial homoclinic orbits. By a different method, it was recently shown that localized states in variational systems are intimately related to Maxwell points, and thus nonpropagating fronts, connecting either two uniform states [8] or a uniform and a periodic [9] state. In the second case, there can be an effective broadening of the Maxwell point so that stationary fronts exist over a finite parameter range [10]; this phenomenon is referred to as *pinning*.

While biological patterns have been extensively studied in the context of periodic patterns [3], there is no unified theory of coherent states (localized and fronts) and the resulting spatiotemporal dynamics in systems that involve autocatalytic saturation [11]. On the other hand, the effect of front asymmetry in the context of formation mechanisms of localized states is also unclear [6]. To advance these issues, we study the formation and the interaction mechanisms of coherent states, holes, peaks and fronts, in a biological activator-inhibitor prototype model. We show that the known phenomenon of *continuous branch pinning* (CBP) can also be found in dissipative systems. In addition, we present a type of pinning, to which we refer as *discontinuous branch pinning* (DBP). In case of CBP, the existence region of holes, which is below the Turing onset, is disjunct from the region of peaks, which is near the bistability saddle-node of the uniform states. As the control parameter is varied, the Turing onset approaches the saddle-node, and the regions of holes and peaks overlap. This overlap results in the formation of a DBP structure of holes via the time-independent front (hetoroclinic bifurcation), which in turn also separates regions of counterpropagating asymmetric fronts. As a consequence, front counter-propagation and the existence of localized states give rise to an intriguing behavior: activator domain growth or contraction accompanied by a simultaneous formation of embedded localized axisymmetric or striped states, as shown in Fig. 1.

We start with a phenomenological activator-inhibitor model introduced by Gierer and Meinhardt [12], to study biological pattern formation. Our interest in this model stems from calcification in vascular-derived mesenchymal stem cell (VMSC) cultures [13], cells that are considered to be responsible for cardiovascular calcification [14]. In particular, it is assumed from biochemistry that the activator obeys a saturated autocatalytic reaction [15] and promotes production of the inhibitor [16]. The cells also express a rapidly diffusing inhibitor [13]. This biochemical activator-inhibitor dynamics therefore qualitatively rationalize the framework of Gierer-Meinhardt model [5, 12], which in its dimensionless form reads [17]

$$\begin{aligned} \frac{\partial u}{\partial t} &= D\nabla^2 u + \frac{u^2 v^{-1}}{1+u^2} - u\,, \\ \frac{\partial v}{\partial t} &= \nabla^2 v + Pu^2 - Ev + S, \end{aligned} \tag{1}$$

where $u(x,y)$ is activator, $v(x,y)$ is inhibitor, D is the diffusion ratio, P represents the generalized cross reaction rates

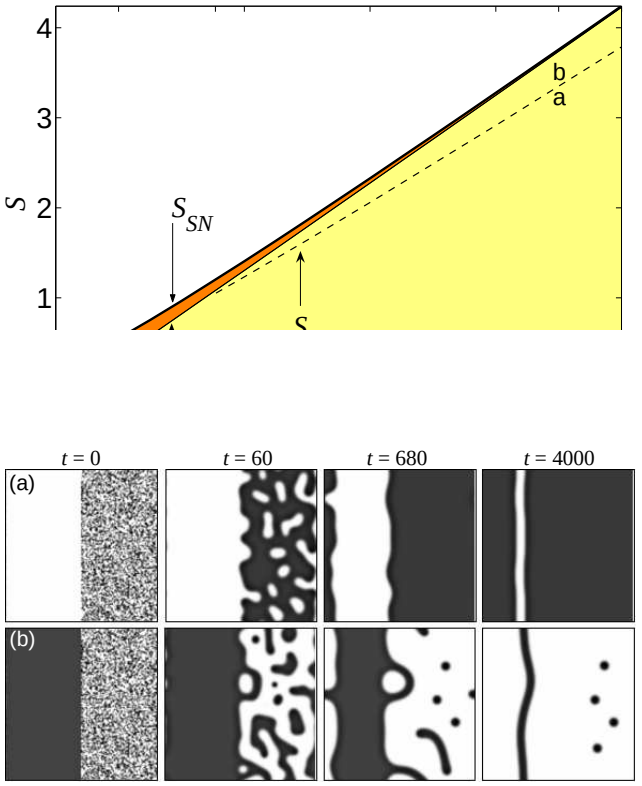

FIG. 1: (Color online) Top panel: Bistability region, $S < S_{SN}$, of uniform solutions $(0, v_0)$ and (u_+, v_+) in the $E - S$ plane (shaded region). The dark shaded region, $S_T < S < S_{SN}$, marks the linear instability of the uniform (u_+, v_+) state to nonuniform perturbations, where S_T is the onset of Turing instability. The dashed line $S = S_M$, for $E > E_c \simeq 3.54$, represents the stationary front between $(0, v_0)$ and (u_+, v_+) states (heteroclinic bifurcation). For $S < S_M$, (u_+, v_+) invades $(0, v_0)$ while for $S_M < S < S_T$ $(0, v_0)$ invades (u_+, v_+). Bottom panel: Demonstration of the activator (a) expansion and (b) contraction process at marked locations in the left panel, stationary front $S = S_M \simeq 3.35$ for $E = 9$, via numerical integration of Eq. (1) on $x = y = [0, 15]$ domain with periodic boundary conditions. The frames show a gray-scale map of the u field, where black denotes a high value of u. The initial condition is either uniform (a) $u = 0.01$ or (b) $u = 1$ in the left half of the domain, while the right half is a uniform random distribution between 0.01 and 1. Parameters: (a) $S = 3.3$, (b) $S = 3.4$, and for both $P = 1$, $D = 0.005$.

ratio, E is the degradation ratio and S is the generalized inhibitor source term. Due to the interest in vascular calcification [14], we chose here the parameters estimated in [13] (see supporting online supplement), i.e., $P \sim \mathcal{O}(1)$, $D \sim \mathcal{O}(10^{-2} - 10^{-3})$, and focus on the two remaining parameters S and E, which are experimentally accessible. We note that localized peaks have also been studied in other forms of Eq. (1), in 1D and 2D [11, 18].

Equation (1) admits three uniform solutions, one of which $(u, v) = (0, v_0) \equiv (0, S/E)$ is trivial, and two nontrivial $(u, v) = (u_\pm, v_\pm)$ [19]. Uniform (u_-, v_-) states appear as unstable states from $S = 0$ and annihilate with the stable (u_+, v_+) branch at a saddle-node bifurcation, $S = S_{SN}$, creating *asymmetric* bistability between $(0, v_0)$ and (u_+, v_+) for $0 < S < S_{SN}$. A primary requirement for both stable localized and front solutions is the linear stability of the uniform solutions to nonuniform perturbation. Standard linear analysis of $(0, v_0)$ and (u_+, v_+) yields that only the nontrivial state goes through a Turing instability at $S = S_T$. The unstable Turing region $S_T < S < S_{SN}$ shrinks by approaching the saddle-node bifurcation, $S = S_{SN}$, as the degradation ratio E is increased (see Fig. 1). Consequently, stable front solutions connecting the uniform (u_+, v_+) and $(0, v_0)$ states exist below $S = S_T$.

Next, we study the properties of localized states via *spatial dynamics* [20] followed by numerical branch continuation method [21] and temporal eigenvalue numerical analysis to determine stability. We set $\partial_t u = \partial_t v = 0$ and analyze (1) as a reversible fourth order ordinary differential equation due to the $x \to -x$ invariance. Linearizations about the uniform states result in steady state solutions which are proportional to $\exp(\lambda x)$, where the spatial eigenvalue λ satisfies a fourth order algebraic equation. For the (u_+, v_+) case, three possible solutions for λ in complex phase space arise: (*i*) for $S > S_T$ the eigenvalues split on the imaginary axis; (*ii*) for $S < S_T$ they split and form a complex quartet; and (*iii*) at the Turing onset, $S = S_T$, a double multiplicity of pure imaginary eigenvalues $\lambda = \pm i k_T$ is present, where k_T is the critical Turing mode. Thus, localized states that exponentially asymptote to (u_+, v_+) can be expected to arise for $S < S_T$ [9]. On the other hand, linearization about $(0, v_0)$ yields four real eigenvalues, $\lambda = \pm\sqrt{E}$ and $\lambda = \pm\sqrt{D^{-1}}$. Thus, localized states that exponentially asymptote to $(0, v_0)$ are expected to arise everywhere. For finite values of E, effective bifurcation of these states is at the transcritical onset, $S = 0$ (the mechanism will be discussed elsewhere). In the following, we refer to L^+ as "holes" while to L^0 as "peaks" in the background of the nontrivial and trivial activator fields, respectively.

To study the localized solutions *far* from the onset, we implement a numerical branch continuation method [21]; the results are presented as a function of S in terms of the norm

$$N = \sqrt{\frac{1}{L}\int_0^L \left[u^2 + v^2 + (\partial_x u)^2 + (\partial_x v)^2\right] \mathrm{d}x}\,, \qquad (2)$$

where L is the spatial period; the domain size used in our numerical calculations is much larger than the spatial period $2\pi/k_T$. We distinguish between two qualitatively distinct regions (see Fig. 1): $E < E_c$, where the holes and peaks do not overlap, and $E > E_c$ (see Fig. 2), where peaks and holes regions do overlap, and reconnect at $S = S_M$ via the stationary heteroclinic cycle between (u_+, v_+) and $(0, v_0)$ (see Fig. 3).

First, we discuss the $E < E_c$ case. Localized hole solutions, L^+, and periodic Turing states (not shown) bifurcate subcritically as unstable small amplitude states [17], from the Turing onset, $S = S_T$, and form a CBP region (shaded region in Fig. 2), as also happens in variational systems [9]. Since the localized holes bifurcate from a nontrivial state, only two even parity solutions with phase shifts of π can form. Thus, we termed a branch with an odd number of holes as L_0^+ [Fig. 2(a)] and the one with an even number as L_π^+ [Fig. 2(b)].

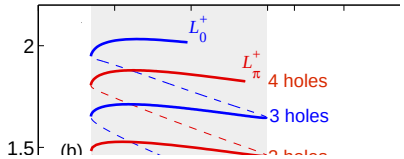

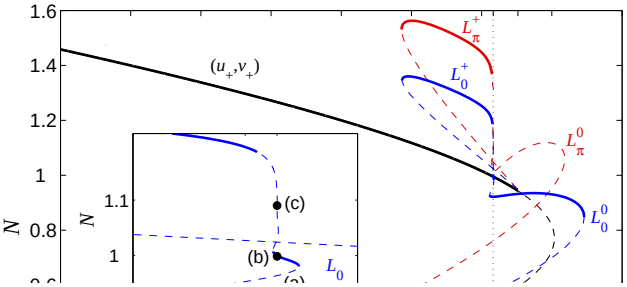

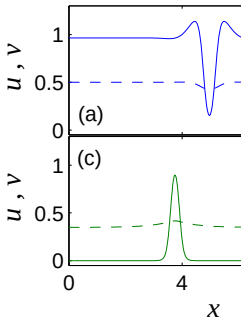

FIG. 2: (Color online) To
1D, showing the norm (2)
and localized states: L_0^+,
stable (unstable) solution
region. S_T and S_{SN} cor
(see text for details), resp
(dashed) profiles at locati
The saddle-nodes and th
branches agree with the st
(a,b) $S \simeq 0.071$ (c) $S \simeq$
$D = 0.005$, $P = 1$.

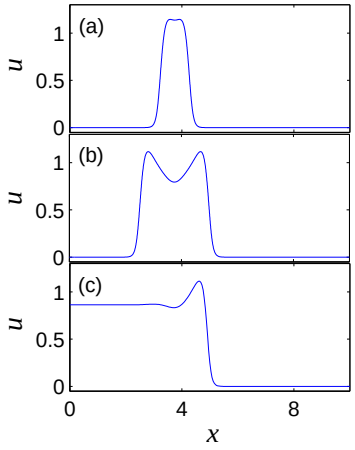

FIG. 3: (Color online) Top panel: Bifurcation diagram for $E = 4$ (solid (dashed) lines mark stable (unstable) solutions). The inset in the top panel clarifies the behavior of L_0^+ and L_0^0 branches at $S = S_M \simeq 1.233$. Bottom panels: Profiles of u at locations indicated in the inset. Note the asymmetry of the heteroclinic orbit (half of the cycle) in (c). Other parameters as in Fig. 2.

Each stable branch of odd and even hole solutions (inside the shaded region) indicate increasing (with N) number of holes [9]. Here we used a relatively small domain which limits further excursions of the two branches (Fig. 2), while on an infinite domain, the branches contain an infinite number of saddle-node points. On the other hand, the localized states that are homoclinic to the $(0, v_0)$ state effectively bifurcate from $S = 0$ and do not form a pinning region, due to real eigenvalues. These states contain only a single stable branch of L_0^0 while the other even branch L_π^0 is unstable [see profiles (c,d) in Fig. 2], denoting a repulsive interaction between two neighboring peaks. Here the subscripts 0 and π, are artificial notations.

Next, we turn to a discussion of the second case, $E > E_c$. We showed in Fig. 1, that an increase in E results in $S_T \to S_{SN}$. Above $E = E_c \simeq 3.54$, this shift causes an overlapping between the CBP region of hole states and the peak states that are present near the saddle-node $S = S_{SN}$. This hole-peak interaction allows formation of a time-independent asymmetric front (via heteroclinic bifurcation) at $S = S_M$, connecting the trivial and the nontrivial states (see Fig. 3). All the localized state branches that were present in the $E < E_c$ case, now effectively collapse nonmonotonically at $S = S_M$. The single and the double hole state, $L = L^+$, still bifurcate from the Turing onset (see Fig. 3), but all other branches (not shown here for simplicity) arise from and reconnect after a single excursion, back to $S = S_M$. This DBP region is structurally different from the classical CBP, described for $E < E_c$ and in [9]. The L^0 branches also go through a significant change: while L_π^0 remains unstable, the L_0^0 branch exhibits decreasing oscillations around $S = S_M$ (see inset of Fig. 3). This behavior is known to give rise to additional localized states [8, 22], with weak spatial oscillations around the primary peak [see Fig. 3(b)].

The activator expansion or contraction and formation of isolated stripes and axisymmetric localized states (Fig. 1) is now transparent. The effective merging point, $S = S_M$, separates regions of counterpropagating single fronts. Thus, opposite front velocities and the simultaneous presence of stable localized holes, peaks and stripes, result in a nontrivial behavior for bistable nonvariational systems with a broken parity symmetry of fronts [see Fig. 3(c)]. In the absence of localized states, the system converges to a finite uniform activator state, a phenomenon that is qualitatively similar to coarsening in variational systems [7]. An additional important aspect

is the stability of coherent structures to curvature and transverse perturbations in 2D. While stability thresholds of localized states may indeed change in 2D, the 1D analysis delimits the regions where stable localized states can also be obtained in 2D [17, 22]. By contrast, instability to transverse perturbations of the front solutions or large circular domains may lead to the formation of periodic patterns that resemble periodic patterns arising from the Turing instability [23]. In our parameter range these fronts are transversally stable, but we cannot exclude the existence of transverse instabilities in general.

We have demonstrated a mechanism for the expansion and contraction of activator domains, and the respective formation of localized states, in a bistable activator-inhibitor system with saturated autocatalysis (Fig. 1). This mechanism stems from the formation of an asymmetric heteroclinic orbit (at a critical parameter value), merging the branches of both hole and peak states. Turing instabilities are found to be important for such behavior, and also for a discontinuous branch pinning structure, as shown in Fig. 3. Since we used global bifurcation methods, we expect similar scenarios to arise in other bistable systems as well, precisely for the same reason that pinning [9] is found in variational models and in our dissipative system. Furthermore, our theoretical results suggest a distinct spatiotemporal behavior in biological systems exhibiting saturation [5]. The concept of activator contraction has potential biomedical applications, for example, localized activator-induced "nodules" are common in biomedicine, such as spotty formations in atherosclerotic calcification [24]. The ability to produce conditions of "activator contraction" to reduce or eliminate these localized spots, therefore has intriguing therapeutic possibilities.

We thank L.L. Demer, Y. Tintut, K. Boström, E. Knobloch, and J. Burke for stimulating discussions.

[1] M.C. Cross and P.C. Hohenberg, Rev. Mod. Phys. **65**, 851 (1993); P.K. Maini, K.J. Painter, and H.N.P. Chau, J. Chem. Soc., Faraday Trans. **93**, 3601 (1997).

[2] A. Turing, Philos. Trans. R. Soc. London, Ser. B **237**, 37 (1952).

[3] S. Kondo and R. Asai, Nature (London) **376**, 765 (1995); K.J. Painter, P.K. Maini, and H.G. Othmer, Proc. Natl. Acad. Sci. **96**, 5549 (1999); M.P. Harris *et al.*, Proc. Natl. Acad. Sci. **102**, 11734 (2005); S. Sick, S. Reinker, J. Timmer, and T. Schlake, Science **314**, 1447 (2006); M. Yamaguchi, E. Yoshimoto, and S. Kondo, Proc. Natl. Acad. Sci. **104**, 4790 (2007); J.D. Murray, *Mathematical Biology* (Springer, New York, 2002).

[4] J. von Hardenberg, E. Meron, M. Shachak, and Y. Zarmi, Phys. Rev. Lett. **87**, 198101 (2001); Y.-J. Li *et al.*, Science **291**, 2395 (2001); J.H.E. Cartwright, J. Theor. Biol. **217**, 97 (2002); A. Yochelis *et al.*, SIAM J. Appl. Dyn. Syst. **1**, 236 (2002).

[5] A.J. Koch and H. Meinhardt, Rev. Mod. Phys. **66**, 1481 (1994).

[6] E. Knobloch, Nonlinearity **21**, T45 (2008).

[7] P. Coullet, Int. J. Bifurcation Chaos **12**, 2445 (2002); L.M. Pismen, *Patterns and Interfaces in Dissipative Dynamics* (Springer-Verlag, Berlin Heidelberg, 2006).

[8] J. Knobloch and T. Wagenknecht, Physica D **206**, 82 (2005).

[9] P.D. Woods and A.R. Champneys, Physica D **129**, 147 (1999); P. Coullet, C. Riera, and C. Tresser, Phys. Rev. Lett. **84**, 3069 (2000); J. Burke and E. Knobloch, Phys. Rev. E **73**, 56211 (2006).

[10] Y. Pomeau, Physica D **23**, 3 (1986).

[11] T. Kolokolnikov, W. Sun, M. Ward, and J. Wei, SIAM J. Appl. Dyn. Syst. **5**, 313 (2006).

[12] A. Gierer and H. Meinhardt, Kybernetik **12**, 30 (1972).

[13] A. Garfinkel *et al.*, Proc. Natl. Acad. Sci. **101**, 9247 (2004).

[14] Y. Tintut *et al.*, Circulation **108**, 2505 (2003); K.A. Hruska, S. Mathew, and G. Saab, Circ. Res. **97**, 105 (2005); J.-S. Shao, J. Cai, and D.A. Towler, Arterioscler., Thromb., Vasc. Biol. **26**, 1423 (2006).

[15] N. Ghosh-Choudhury *et al.*, Biochem. Biophys. Res. Commun. **286**, 101 (2001).

[16] A. F. Zebboudj, V. Shin and K. Boström, J. Cell Biochem. **90**, 756 (2003).

[17] A. Yochelis, Y. Tintut, L.L. Demer, and A. Garfinkel, e-print arXiv:nlin.PS/0712.3780.

[18] A. Doelman and H. van der Ploeg, SIAM J. Appl. Dyn. Syst. **1**, 65 (2002); M. Ward *et al.*, SIAM J. Appl. Math. 62, 1297 (2002).

[19] For $P = 1$, $[u_\pm, v_\pm] = [(\sqrt{\theta} \pm \sqrt{\eta})/2, \sqrt{\theta}(\sqrt{\theta} \pm \sqrt{\eta})/(E - (S-1)\sqrt{\theta} \pm \theta\sqrt{\eta})]$, where $\eta \equiv 2E/\sqrt{\theta} + \phi$, $\theta \equiv \beta/3\rho + \rho/3 - 2(S+1)/3$, $\phi \equiv -\theta - 2(S+1)$, $\rho \equiv (\alpha/2 + \sqrt{\alpha^2/4 - \beta^3})^{1/3}$, $\alpha \equiv 27E^2 - 72S(S+1) + 2(S+1)^3$, $\beta \equiv 1 + 14S + S^2$.

[20] A.R. Champneys, Physica D **112**, 158 (1998).

[21] E. Doedel *et al.*, *AUTO2000: Continuation and bifurcation software for ordinary differential equations (with HomCont)*, http://indy.cs.concordia.ca/auto/.

[22] A. Yochelis, J. Burke, and E. Knobloch, Phys. Rev. Lett. **97**, 254501 (2006).

[23] A. Hagberg and E. Meron, Chaos **4**, 477 (1994); R.E. Goldstein, D.J. Muraki, and D.M. Petrich, Phys. Rev. E **53**, 3933 (1996); D. Gomila, P. Colet, G.-L. Oppo, and M. San Miguel, J. Opt. B: Quantum Semiclassical Opt. **6**, S265 (2004); A. Yochelis, C. Elphick, A. Hagberg, and E. Meron, Physica D **199**, 201 (2004).

[24] M. Abedin, Y. Tintut, and L.L. Demer, Arterioscler., Thromb., Vasc. Biol. **24**, 1161 (2004).